The effect of change in soil volume on organic matter distribution in a volcanic ash soil

Tonneijck, F.H.; Velthuis, M.; Bouten, W.; van Loon, E.E.; Sevink, J.; Verstraten, J.M.

Citation for published version (APA):
Tonneijck, F. H., Velthuis, M., Bouten, W., van Loon, E. E., Sevink, J., & Verstraten, J. M. (2016). The effect of change in soil volume on organic matter distribution in a volcanic ash soil. *European Journal of Soil Science*, *67*(2), 226-236. https://doi.org/10.1111/ejss.12329

The effect of change in soil volume on organic matter distribution in a volcanic ash soil

F. H. T o n n e i j c k, M. V e l t h u i s, W. B o u t e n, E. E. V a n L o o n, J. S e v i n k &
J. M. V e r s t r a t e n
Institute for Biodiversity and Ecosystem Dynamics, University of Amsterdam, Amsterdam, 1098XH, The Netherlands

Summary

Volcanic ash soil contains large stocks of organic matter per unit area. A large proportion of organic matter is stored in the subsoil; therefore, a thorough understanding of its vertical distribution is needed to predict the effects of change in climate and land use. Faunal bioturbation is often cited as the dominant process that affects the vertical distribution of organic matter. An additional but often overlooked process is change in the volume of the soil. Such change might affect the vertical distribution of organic matter by changing the position of the soil surface, which can affect the soil-forming processes related to depth, such as weathering, decomposition, bioturbation and rooting. We calculated the change in volume with geochemical mass balance equations, and showed the effect of change in soil volume on the vertical distribution of organic matter using a dynamic model. Then we evaluated the plausibility of the model concept with an independent model for parameter identification and through a model sensitivity analysis. Results show that volume change is a major soil-forming process that determines the vertical distribution of organic matter in volcanic ash soil as the active bioturbation zone moves upwards in response to soil thickening.

Highlights

- The research addresses how the vertical distribution of organic matter is affected by change in soil volume.
- The effect of change in volume on SOM distribution is important in SOM-rich soil and overlooked in models of carbon dynamics.
- Soil volume tripled over 4800 years, influencing bioturbation and consequently vertical SOM distribution.
- Change in soil volume cannot be disregarded when modelling and interpreting SOM distribution in SOM-rich soil.

Introduction

Soil organic matter (SOM) constitutes the largest pool of terrestrial organic carbon. Soil is a potential source and sink of the greenhouse gas CO_2, which is of global importance (Batjes, 1996; Lal, 2004). This is reflected in global models for carbon cycling that incorporate SOM dynamics. Most models of SOM dynamics focus on the topsoil (< 25-cm depth) and disregard the subsoil. However, a large fraction of SOM is stored in the subsoil, where its stability against decomposition is supposedly greater. A thorough understanding of the processes that affect the vertical distribution of SOM is needed to predict the effects of changes in climate and land use on the

stocks of carbon (Elzein & Balesdent, 1995; Jobbágy & Jackson, 2000; Jenkinson *et al.*, 2008). The vertical distribution of SOM in volcanic ash soil merits special attention because such soil (mainly Andosols) typically contains large stocks of SOM per unit area (Batjes, 1996; Lal, 2004). Although volcanic ash soil covers about 1% only of the world's land area, it contains about 5% of the global soil carbon (Dahlgren *et al.*, 2004). Consequently, the effects of changes in climate and land use on SOM in volcanic ash soil might be strong.

The vertical distribution of SOM in soil is determined by (i) input of litter, above and below ground, (ii) decomposition and (iii) vertical transport. In volcanic ash soil, deposition of fresh volcanic material (tephra) also affects the vertical distribution of SOM. With respect to vertical transport, faunal bioturbation (further referred to simply as 'bioturbation') is an important process.

Elzein & Balesdent (1995) demonstrated in a modelling study that bioturbation is more important than leaching in several types of soil. Leaching of SOM is insignificant in volcanic ash soil because of large metal-to-SOM ratios that result in immobilization of SOM in organo-metallic complexes (Aran *et al.*, 2001; Dahlgren *et al.*, 2004).

An additional process, change in soil volume, that is often overlooked might also affect the vertical distribution of SOM. Soil can collapse or thicken during its formation because of a loss of chemical elements during weathering, incorporation of organic matter through bioturbation or a change in porosity, for example caused by biological activity or swelling and shrinking (Douglas & McKyes, 1978; Chadwick *et al.*, 1990; Blanco-Canqui *et al.*, 2006; Rühlmann *et al.*, 2006). Because volume change affects the position of the soil surface (relative to the soil base), it also influences soil-forming processes related to soil depth (relative to the soil surface), such as weathering, decomposition, bioturbation and rooting. Figure 1 shows how soil thickening might cause the active bioturbation zone to shift upwards over time relative to the soil's base. Volume change is taken into account in models of soil genesis (Chadwick *et al.*, 1990; Salvador-Blanes *et al.*, 2007), but to our knowledge it has not been taken into account previously in models that deal specifically with the dynamics of organic carbon. The effect of change in soil volume on the vertical distribution of SOM, however, might be substantial, particularly in soil rich in organic matter.

We aimed to demonstrate the effect of volume change on the vertical distribution of organic matter in a volcanic ash soil. To achieve this, first we calculated the degree of change in soil volume with geochemical mass balance equations. Second, we modelled the effect of change in soil volume on the vertical distribution of SOM with a dynamic model. Third, we evaluated the plausibility of our model concept with an independent model for parameter identification and by a model sensitivity analysis.

Description of study area and sites

The study area is in the nature protection area of Guandera Biological Station in northern Ecuador, near the border with Colombia. For the current study, we selected a site (G7, N 0°35′48″/W 77°41′25″) at 3860 m above sea level (a.s.l.) that has been covered by páramo vegetation for the last few thousands of years (Bakker *et al.*, 2008). Dominant species in the páramo are bunch-grass *Calamagrostis effusa* Kunth (Steud.) and stem rosette *Espeletia pycnophylla* Cuatrec. The páramo ecosystem

Figure 2 Photograph of the soil profile studied.

belongs to the Tropical Andes biodiversity 'hotspot' according to Myers *et al.* (2000). A biodiversity hotspot is a biogeographic region with a considerable reservoir of biodiversity that is under threat from human activity. Mean annual precipitation is around 1900 mm and mean annual temperature ranges from 12°C at 3000 m a.s.l. to 4°C at 4000 m a.s.l. Both precipitation and temperature show little seasonal variation. The soil's climate, according to USDA's Soil Survey Staff (2015), is isomesic (between 8 and 15°C, with a difference between mean summer and winter temperatures of less than 6°C) and perudic (a very wet regime in climates where precipitation exceeds evapotranspiration in all months in most years).

The soil profile has formed in three tephra deposits of Holocene age (Tonneijck *et al.*, 2008) (see Figure 2). The timing of the last
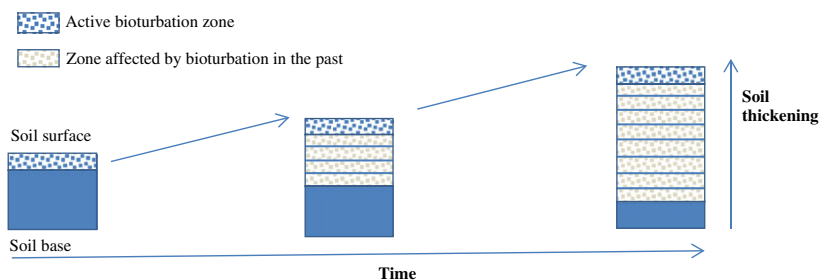

Figure 1 Volume change affects the position of the surface, resulting in an upwardly moving bioturbation zone. Rooting and weathering zones might also move upwards.

tephra deposit was estimated by calibrated radiocarbon dating at 2779 cal BC (Tonneijck *et al.*, 2008), resulting in ~4800 years of soil formation. Related to this tephra stratigraphy, the soil contained a current soil, a palaeosol and a second heavily truncated or immature palaeosol, each at least 40-cm thick. The main focus of this research was on the current soil profile. Above-ground litter is present mainly as hanging dead material in the tussock grasses or on the stem rosettes rather than in a litter layer. The bottom of the current soil and the top of the first palaeosol show signs of mixing in the form of atypical organic carbon contents, grain sizes and chemical element ratios. In the soil horizon designations, we use '1/2' as a prefix to indicate this transitional zone. A thin placic horizon is present at the boundary between the first and second palaeosol, which is ascribed to a strong textural contrast that hinders drainage of the otherwise well-drained soil. The soil is an Andosol according to the World Reference Base (FAO, 2006).

Materials and methods

For a glossary of symbols and indices, see Table 1.

Sampling and laboratory procedures

The data used have been presented by Tonneijck *et al.* (2008) and Tonneijck & Jongmans (2008). We discuss only briefly the sampling and laboratory procedures here. We took soil samples for physical and chemical analyses and ring samples for the estimation of soil dry bulk density. Samples were taken in the same soil pit at regular depths, but we avoided sampling at horizon boundaries. In addition, we took undisturbed vertical soil samples (monoliths) with metal gutters of 75-cm length $\times$ 5-cm width $\times$ 4-cm depth. For additional estimates of organic carbon contents, sample cores were taken from these monoliths by means of a corer of 0.75-cm diameter. All samples were stored at 2°C under field-moist conditions.

Total carbon was measured with a VarioEL (Elementar, Hanau, Germany) CNS auto-analyser. Total carbon represents organic carbon because carbonates were absent. We assumed that SOM content was twice the amount of total organic carbon content according to Van Reeuwijk (2002), and we use both terms interchangeably. We determined dry bulk density by weighing oven-dried samples of soil of known volume of 100 cm^3 (dried at 105°C until constant weight was reached after > 24 hours). Concentrations of the immobile elements Ti and Al were estimated with a Perkin Elmer Optima 3000 XL ICP-OES (Waltham, MA, USA) in ground, dried and heated (900°C) samples ($n = 4$ for current soil and top of the transitional zone and $n = 13$ for the reference material) after destruction in a hot mixture of hydrofluoric (HF) and sulphuric (H$_2$SO$_4$) acids.
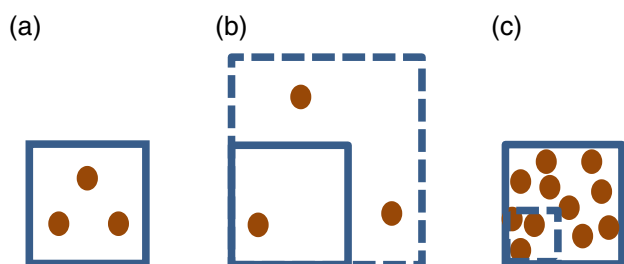
Volume change

Elements that are immobile during soil formation, for example titanium (Ti) and in the case of Andosols also aluminium (Al), can be used to reconstruct soil volume before weathering has occurred (see Figure 3). Reconstruction of the volume before weathering is needed to determine change in soil volume over time.

To calculate volume change we followed the approach of Brimhall & Dietrich (1987) and Chadwick *et al.* (1990) and used the strain equation. In this case, strain represents a change in thickness over time:

Table 1 Glossary of symbols and indices

Symbol	Description	Symbol	Description
a_1	Slope of the linear function	σ	Standard deviation
a_2	Intercept of the linear function	τ	Transport, the mass fraction of a mobile element added to or subtracted from the system
C	Mass percentage (%)	t	Time (year)
c_1	Constant	U	Unit area (cm^2) of modelled soil column
c_2	Constant	w	Parameter (cm^{-1}) influencing the width of Gaussian kernel
D	Diffusion coefficient (cm^2 year^{-1})	x	Soil depth (cm), measured from the soil surface downwards
ε	Change in soil thickness expressed as strain (cm cm^{-1})		
f	Mass fraction (g g^{-1})	**Index**	**Description**
g	A distribution parameter, chosen such that 80% of root litter input is contained in the top 10 cm of soil	A	Bioturbation type A (epigeic species)
h	A small $D(x)$ value beyond which the bioturbation is set at zero	B	Bioturbation type B (endogeic species)
I	Input (g year^{-1})	b	Bulk
k	Relative decay (year^{-1})	i	Immobile element
L	Thickness (cm) of a layer	j	Mobile element
m	Mass (g)	r	Reference material
Q	Percentile	s	Solids
R^2	Coefficient of determination	w	Weathered material
ρ	Density (g cm^{-3})	–	–

Figure 3 Immobile elements were used to calculate change in soil volume. (a) Original situation with reference concentration of immobile elements and reference bulk density. (b) Soil formation resulting in soil thickening: for the same amount of stable elements there is now a larger soil volume; bulk density less than in reference. (c) Soil formation resulting in soil collapse: for the same amount of stable elements there is now a smaller soil volume; bulk density greater than in reference.

$$\varepsilon_i\left(x, t_{end}\right) = \frac{{}^b\rho_{s,r}\, C_{i,r}}{{}^b\rho_{s,w}\left(x, t_{end}\right) C_{i,w}\left(x, t_{end}\right)} - 1, \qquad (1)$$

where $\varepsilon_i(x,t_{end})$ in (cm cm^{-1}) is the change in thickness (strain) at $t_{end} = 4800$ (year) over initial thickness at $t_0 = 0$ (year) from soil formation, at depth x (cm) with subscript i that refers to the use of an immobile strain index element. Furthermore, ${}^b\rho_{s,r}$ and ${}^b\rho_{s,w}$ represent the soil dry bulk density (g cm^{-3}) of the reference soil material (subscript r) and weathered material (subscript w), respectively, and $C_{i,r}$ and $C_{i,w}$ represent the mass percentage (%) of immobile element i in the reference material and weathered material, respectively. We used a fairly unweathered second palaeosol derived from various soil pits in the study area as the reference material (3BCb horizon, Table 2).

We measured dry soil bulk density and immobile element concentrations at four sampling depths, and regressed change in soil thickness (strain) on soil depth x (Figure 4) to determine initial

thickness of the current soil more accurately (Equation (3)):

$$\varepsilon_i\left(x, t_{end}\right) = a_1 x + a_2. \qquad (2)$$

Parameters a_1 and a_2 are given in the captions of Figure 4(a,b). The R^2 values of these linear regressions exceeded 0.92 in all cases.

To calculate the initial thickness at t_0 of the entire current soil (i.e. before volume change) we applied Equation (2):

$$L\left(x, t_0\right) = \frac{L\left(x, t_{end}\right)}{1 + \varepsilon\left(x, t_{end}\right)} = \frac{1}{1 + a_1 x + a_2}$$

and

$$L_{current}\left(t_0\right) = \int_{x_{top}}^{x_{current}} L\left(x, t_0\right) dx$$
$$= \frac{1}{a_1} \ln\left(a_1 x_{current} + a_2 + 1\right) - \ln\left(a_2 + 1\right), \qquad (3)$$

where $L(x,t_0)$ represents the initial thickness (cm) of a layer and $L(x,t_{end})$ represents the thickness of this layer after soil formation, which we set arbitrarily at 1 cm. The total thickness observed of the entire current soil at t_{end} is 77 cm and is referred to as $L_{current}(t_{end})$. The latter is the thickness from the mineral soil surface (x_{top}) to the middle of the transitional zone ($x_{current}$). The quantity $L(x,t_0)$ was integrated from x_{top} to $x_{current}$ to obtain the initial thickness of the entire current soil (i.e. $L_{current}(t_0)$). We computed minimum and maximum $L_{current}(t_0)$ from minimum and maximum values of strain, and used $L_{current}(t_0)$ as input to our model.

Correct application of this technique depends on immobility during weathering of at least one element; otherwise pre-weathering soil volume cannot be reconstructed accurately. We used Ti and Al as probable immobile elements to evaluate internal consistency. Furthermore, immobility of an element can be checked against another supposedly immobile element and vice versa by calculating

Table 2 Soil properties of samples from the soil profile studied and of reference material (3BCb horizons) taken from various locations in the study area ($n > 8$; standard deviations, σ, are reported)

Horizon[a]	Depth / cm	C / mass %	σ	Bulk density / g cm^{-3}	σ	Soil pH$_{CaCl_2}$	σ	TiO$_2$ / mass %	σ	Al$_2$O$_3$ / mass %	σ
Ah1	10	20.1		0.35		3.92		0.33		10.4	
Ah1	30	16.3		0.40		4.10		0.37		11.9	
Ah2	47	12.7		0.42		4.30		0.43		13.9	
1/2Ah2	63	13.5		0.41		4.34		0.49		14.7	
1/2Ahb	90	19.6		0.34		4.16		0.57		14.0	
2Ahb	110	15.6		0.39		4.24		0.64		15.7	
2Bwb	140	5.3		0.71		4.56		0.71		19.9	
2Bsb	148	3.8		–		4.88		0.57		16.1	
3BCb	154	2.7		–		4.84		0.67		19.7	
3BCb	170	0.4		0.93		5.36		0.70		19.9	
Reference material	–	0.81 ($n = 15$)	1.11	0.95 ($n = 8$)	0.04	5.11 ($n = 15$)	0.32	0.66 ($n = 13$)	0.10	19.31 ($n = 13$)	0.85

[a]Prefix 1/2 refers to the transition zone; see description of study area and sites.

(a) Strain $\varepsilon_{Ti,w}$

(b) Strain $\varepsilon_{Al,w}$
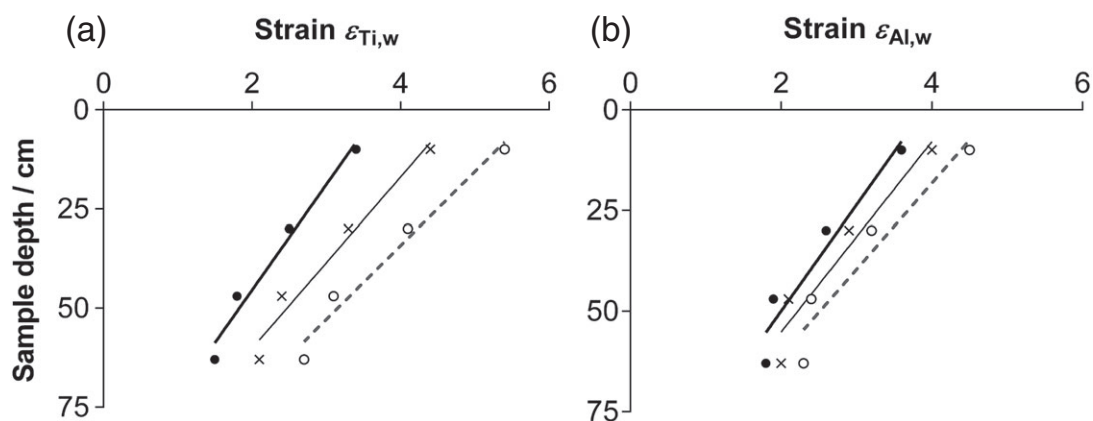
Figure 4 Change in thickness (strain ε) versus sample depth (cm) computed with (a) Ti as immobile index element or (b) Al as immobile index element, applying $\varepsilon_i(x, t_{end}) = a_1 x + a_2$.

- • Minimum strain, with $\varepsilon_{Ti,w} = -0.04x + 3.7$ and $\varepsilon_{Al,w} = -0.04x + 3.8$;
- ○ maximum strain, with $\varepsilon_{Ti,w} = -0.05x + 5.8$ and $\varepsilon_{Al,w} = -0.04x + 4.7$;
- × average strain, with $\varepsilon_{Ti,w} = -0.04x + 4.7$ and $\varepsilon_{Al,w} = -0.04x + 4.2$.

its transport (Chadwick *et al.*, 1990) with:

$$\tau_j\left(x, t_{end}\right) = \frac{{}^b\rho_{s,w}\left(x, t_{end}\right) C_{j,w}\left(x, t_{end}\right)}{{}^b\rho_{s,r} C_{j,r}}\left(\varepsilon_i\left(x, t_{end}\right) + 1\right), \quad (4)$$

where $\tau_j(x, t_{end})$ is the mass fraction of mobile element j added to or subtracted from the system.

Modelling vertical SOM distribution

A flow chart of the dynamic model is given in Figure 5.

General model structure. The soil profile was modelled with a one-dimensional partial differential equation in which we defined layers with initial thickness of 5 cm and an area of 1 cm² in the horizontal plane. Layers varied in thickness to simulate the change in soil volume (see next section). The soil surface (x_{top}) was chosen as the upper boundary of the system and the lower boundary was chosen just above the placic horizon (x_{base}). The model used time-steps of 5 years. We started our model run ($t_0 = 0$) at the moment of the last tephra deposition (i.e. before formation of the current soil) and applied ~4800 years (t_{end}) of soil formation. Organic carbon mass and mineral mass were the state variables of the dynamic system (see Figure 5). We used mass-based units rather than volume-based units because the soil changes volume during simulation. The states were determined by SOM input, SOM output and SOM transport, which are discussed in the next sections. Leaching of mineral mass was assumed to be negligible compared with SOM incorporation and was not simulated as a separate process.

Change in soil volume. Soil volume changed during the model's time-frame from an initial total soil thickness of 20 cm (an estimate based on the above geochemical mass balance calculations) to the 77 cm currently observed. In our model, we varied the thickness of the layers over time to simulate this change in volume during soil formation. At every time-step we recalculated dry soil bulk density of a layer at depth x and year t with an empirical relation between organic carbon content and dry soil bulk density based on data from the same study area (Tonneijck *et al.*, 2008, $R^2 = 0.98$):

$$^b\rho_{s,w}(x, t) = c_1 \exp c_2 f_{OC}(x, t), \quad (5)$$

where $c_1 = 0.9 \, g \, cm^{-3}$, $c_2 = -5.5$ and $f_{OC}(x, t)$ is the mass fraction of organic carbon $g \, g^{-1}$. Because of the exponential nature of the relation between organic carbon and dry soil bulk density, we assumed that this relation reflects the combined effect of all soil-forming processes and not only of SOM incorporation.

Subsequently, dry soil bulk density was used to recalculate the thickness of that layer according to the following equation:

$$L(x, t) = \frac{m_b(x, t)/U}{{}^b\rho_{s,w}(x, t)}, \quad (6)$$

in which $L(x,t)$ is the thickness of a layer, $m_b(x,t)$ is the sum of mineral and SOM mass (g) of that layer and U is the unit area (cm²). Integrating $L(x,t)$ from x_{top} to x_{base} gave $L_{tot}(t)$ for the entire soil profile. Layers that grew beyond a thickness threshold of 10 cm were divided into two equally thick layers.

Input of SOM. In the model, organic carbon entered the soil's above-ground (shoots) and below-ground (roots) litter. We assumed that the annual rate of above-ground litter production was constant, which is a necessary simplification in the absence of data that cover the past millennium. Below-ground litter production was assumed to be proportionate to above-ground litter production; we used the ratio reported by Hofstede & Rossenaar (1995) for the proportion of above- to below-ground biomass. In accord with Elzein & Balesdent
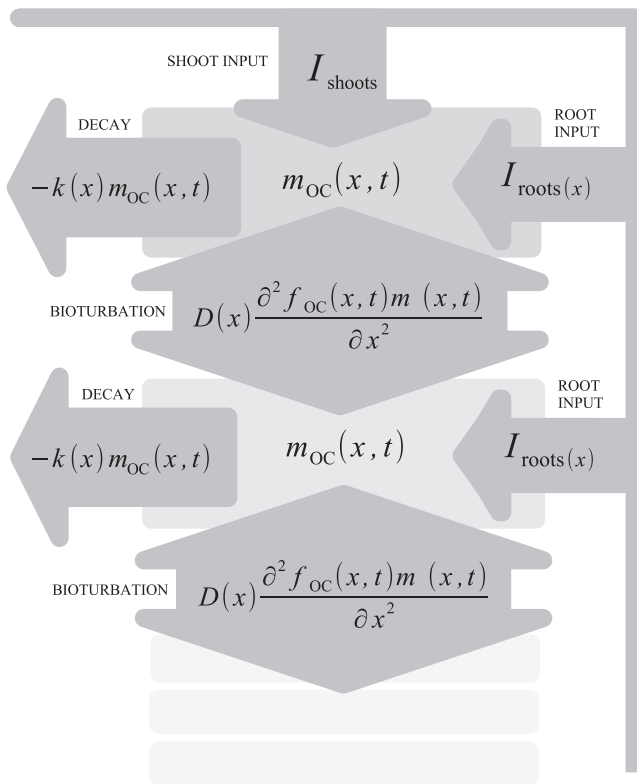
Figure 5 Flow chart of dynamic model. For every time-step the thickness and depth of each layer is recalculated. First, the carbon fraction is calculated and used to derive bulk density. The bulk density, together with the sum of mineral and SOM mass, determines the thickness and thus depth. The newly calculated depths affect depth-dependent processes in the next time-step.

(1995), we assumed that root litter input decreases exponentially with depth x, according to the following equation:

$$I_{\text{roots}}(x) = \frac{I_{\text{shoots}}}{I_{\text{roots}}} I_{\text{shoots}} \frac{\exp(-gx)}{g}, \qquad (7)$$

in which $I_{\text{roots}}(x)$ is organic carbon input by root litter (g year^{-1}), I_{shoots} is organic carbon input by shoot litter (g year^{-1}) and g is a distribution parameter. Rooting is typically shallow in the páramo with ~80% of root biomass within the upper 10 cm of soil (Hofstede & Rossenaar, 1995), and this was also observed in the soil profile studied (Tonneijck & Jongmans, 2008). Therefore, we chose parameter g so that 80% of the total root litter input was in the top 10 cm of the soil.

We assumed that only 'resistant plant material' entered the mineral soil in our model, and that decomposition of other materials is so fast that it does not affect the organic carbon-depth profile at the timescale of our model. We assumed that 10% of the litter was resistant plant material; a rough estimate based on a comparison of the molecular composition of SOM with that of above-ground litter in the soil profile obtained by analytical pyrolysis (Nierop *et al.*, 2007).

The vertical distribution of organic carbon in the current soil at our site has also been affected by the presence of a carbon-rich palaeosol. We calibrated the initial organic carbon-depth profile of the palaeosol at t_0.

Output of SOM. Organic matter is lost from the soil by decomposition. We assumed the decay rate to be directly proportional to the organic carbon mass of a layer with the differential equation:

$$\frac{\mathrm{d}m_{\text{OC}}(x,t)}{\mathrm{d}t} = -k(x)\,m_{\text{OC}}(x,t) \ , \qquad (8)$$

where $m_{\text{OC}}(x,t)$ is the mass of organic carbon (g) and $k(x)$ is a decay constant (year^{-1}). We assumed that this decay constant $k(x)$ is proportional to bioturbation (Equations (9) and (10)).

Transport of SOM. We assumed that bioturbation is the main process responsible for SOM transport in the soils studied, in accord with Tonneijck & Jongmans (2008). Change in the mass of organic carbon for a layer because of transport by bioturbation was modelled with the diffusion equation (Elzein & Balesdent, 1995; Jarvis *et al.* 2010):

$$\frac{\partial m_{\text{OC}}(x,t)}{\partial t} = D(x)\frac{\partial^2 f_{\text{OC}}(x,t)\,m_{\text{b}}(x,t)}{\partial x^2}, \qquad (9)$$

in which $D(x)$ is the diffusion coefficient (cm^2 year^{-1}) of that layer (see also Equation (10)). Tonneijck & Jongmans (2008) showed that in the soils studied, bioturbation was caused by a group of epigeic and a group of endogeic soil faunal species. Bioturbation features of the epigeic group were concentrated in the topsoil and decreased in abundance with depth (type A), whereas, in contrast, bioturbation features of the endogeic group increased with depth and were most abundant in the subsoil (type B). To represent this

observed pattern of bioturbation in the model we used a function based on two Gaussian-shaped kernels to describe the diffusion coefficient D with depth x:

$$D(x) = D_A \exp^{-(x^2)w_A} + D_B \exp^{-(x-x_B)^2 w_B} \quad \text{for } D(x) \geq h \quad (10)$$

and

$$D(x) = 0 \quad \text{for } D(x) < h,$$

where D_A is the height of the first Gaussian kernel (cm^2 year^{-1}), w_A is a parameter (cm^{-1}) influencing the width of the first kernel (reflecting the depth of bioturbation type A), D_B is the height of the second Gaussian kernel (cm^2 year^{-1}), w_B is a parameter (cm^{-1}) influencing the width of the second Gaussian kernel (reflecting the depth of bioturbation type B), x_B is the depth of bioturbation type B (cm) and h is a small value, $D(x)$, beyond which the value of the kernels is set to zero. Because the position of the soil surface changes in response to volume change, Equation (10) was defined relative to the soil surface and simulates an upwardly shifting active bioturbation zone. We assumed that the páramo vegetation colonized the surface immediately after the last tephra deposit, and also that the soil faunal community immediately colonized the tephra deposit according to this bioturbation pattern.

Evaluation of model plausibility and sensitivity

To evaluate our model concept, we used inverse modelling (Bayesian optimization) to identify parameter values of our dynamic model (Vrugt *et al.*, 2003). If the dynamic model described above does not reflect real-world processes then parameters do not converge during the optimization, and posterior parameter values are beyond realistic ranges because parameters compensate for errors in the model structure. Realistic posterior parameter values enhance the confidence in a model concept that describes real processes.

For inverse modelling we used the Shuffled Complex Evolution Metropolis algorithm, SCEM (Vrugt *et al.*, 2003). The SCEM can cope with tens of parameters in parameter identification (Heimovaara *et al.*, 2004). In the current study, eight parameters were optimized. Initial (prior) parameter ranges were based on values in the literature (Table 3) and were wide to allow for a high degree of freedom. The SCEM randomly selects 200 parameter combinations from these initial parameter ranges and the dynamic model is run with these combinations. The parameter combinations that produce the best results relative to the measured data are then used again to select random combinations of parameters. As such, the SCEM runs the dynamic model thousands of times, each time with a different and better combination of parameters. After thousands of runs, these parameter combinations converge to produce similar model outcomes that accord with the measured data. After convergence there are still many parameter combinations that fit the data. Therefore, instead of obtaining one value per parameter, we obtained a range of values for each parameter. For each parameter we report the 10th and 90th percentile values of this range (Q10 and

Q90, respectively), together with the 'optimal fit' in Table 3. This optimal fit has the best root mean squared error, but deviates only marginally from other fits found after convergence. In the figures we show only this optimal fit for clarity, otherwise the multiple fits cloud the measured data.

To test model sensitivity further, we ran the dynamic model with the optimal parameter fit for all parameters except for the one being tested, which we varied manually. We tested the sensitivity of the model to bioturbation rate and bioturbation depth (represented by the diffusion constant and kernel width) and to the extent of change in soil volume (by varying the initial thickness of the current soil).

Results

Volume change

Soil properties are listed in Table 2. We checked the immobility of Al and Ti by evaluating plots of transport of these elements (calculated with strain based on Ti or Al, respectively, as the immobile index element) against strain (see Figure 6(a,b)).

Positive strain values of up to 4.7 in the topsoil and up to 2.1 in the subsoil show that soil volume increased during soil formation throughout the current soil profile. The subsoil sample deviates from the linear regression because the current soil at that depth is mixed with the palaeosol. A linear regression might underestimate volume change in the subsoil somewhat and consequently lead to a slight overestimate of the initial soil thickness. This results in a conservative estimate of volume change. The initial thickness of the entire current soil is estimated to range between 17 and 26 cm (average 21 cm) with Ti as the immobile index element and 20 and 24 cm (average 22 cm) with Al as the immobile index element. Therefore, the current soil (now 77 cm thick to the middle of the transition zone) increased by 300 to 440% in thickness relative to its initial thickness.

Modelling vertical SOM distribution

The output of the model at several moments in time is shown in Figure 7; we included measured SOM data at $t_{end} = 4800$ years. The linear regression between modelled and measured values has an R^2 of 0.97. The model starts with a palaeosol in which carbon content decreased with depth and a fresh tephra deposit containing no carbon on top of it. Gradually, carbon enters the fresh tephra deposit, both from the soil surface by incorporation of fresh organic matter and through transport from the palaeosol upwards. Soil formation continues until we arrive at the atypical SOM distribution observed in the current soil; that is, a decrease in carbon content with depth from the soil surface followed by an atypical increase with depth from the subsoil of the current soil to the top of the palaeosol. In our model this atypical increase was caused mainly by bioturbation B, which was demonstrated by leaving out bioturbation B (see Figure 7, t_{end}).

Table 3 Initial (prior) parameter values, 10th and 90th percentiles (Q10 and Q90) of the model (posterior) parameter values and optimal model fit after convergence of the SCEM compared with data reported in the literature

| Description	Symbol	Initial value		Modelled value		Optimal model fit	Literature data	References
		Minimum	Maximum	Q10	Q90			
Initial total thickness of the current soil / cm	$L_{current}(t_0)$	Fixed at 20					10–30	Geochemical mass balance calculation, this paper
Above-ground input of organic carbon (shoot litter) / $g\,m^{-2}year^{-1}$	I_{shoot}	10	60	46	49	46	10–1000	Hofstede & Rossenaar (1995) and Tonneijck (1999)
Shoot litter : root litter	$\frac{I_{shoot}}{I_{root}}$	Fixed at 1:0.35					1:0.35	Hofstede & Rossenaar (1995)
Resistant plant material / %		Fixed at 10%					10	Personal communication, Nierop (2008)
Turnover time$_A$ / year	$(1/k)$	6250	125 000	72 971	9954	73 780	4500–170 000	Van Dam *et al.* (1997) and Torn *et al.* (1997)
Turnover time$_B$ / year	$(1/k)$	8333	250 000	166 249	24 954	176 583	4500–170 000	Van Dam *et al.* (1997)
Diffusion coefficient, bioturbation A / $cm^2\,year^{-1}$	D_A	0.8	1.6	0.9	1.5	1.0	0.42–15[a,b]	Elzein & Balesdent (1995)[a] Van Dam *et al.* (1997)[b]
Kernel width parameter, bioturbation A / cm^{-1}	w_A	50	600	52	73	56	–	NB this translates into a bioturbation zone of 10–15 cm (2σ) or 5–10 cm (1σ)
Diffusion coefficient, bioturbation B / $cm^2\,year^{-1}$	D_B	0.4	1.2	0.4	0.6	0.4	–	–
Kernel width parameter, bioturbation B / cm^{-1}	w_B	25	300	69	133	112	0–200	NB this translates into a bioturbation zone of 20–40 cm (2σ) or 5–20 cm (1σ)
Depth of bioturbation B / cm	x_B	40	80	55	60	58	60–80	Tonneijck & Jongmans (2008)

The optimal model fit is used in subsequent figures.

Evaluation of concept plausibility and sensitivity

The parameters with the optimal model fit (Figure 7) are given in Table 3 together with their prior and posterior ranges. Parameters with a narrower posterior than prior range were identified more accurately with the available measurements.

The two modelled Gaussian kernels describing bioturbation do not necessarily overlap. Bioturbation type A is somewhat stronger (optimal fit $1.0\,cm^2\,year^{-1}$) than bioturbation type B (optimal fit $0.4\,cm^2\,year^{-1}$). Both types of bioturbation operate over small vertical distances (1σ bioturbation kernel A = 10–15 cm and bioturbation kernel B = 5–20 cm). The model sensitivity for the rate of bioturbation (represented by D_A) and the depth of bioturbation (represented by w_A) of bioturbation type A are shown in Figure 8 (a,b), respectively. Increasing the rate of bioturbation of type A with a fixed depth range results almost in the homogenization of the organic carbon-depth profile of the current soil. If we apply a fixed rate of bioturbation and a small bioturbation depth range (large w_A), organic carbon accumulates in the topsoil rather than the subsoil. In contrast, if we applied a large depth range (small w_A) the organic carbon content was distributed more evenly throughout the soil. If we left out bioturbation type B (see Figure 7 at t_{end}), the model could not predict the organic carbon-depth pattern currently observed. If we correlate the bioturbation pattern with organic
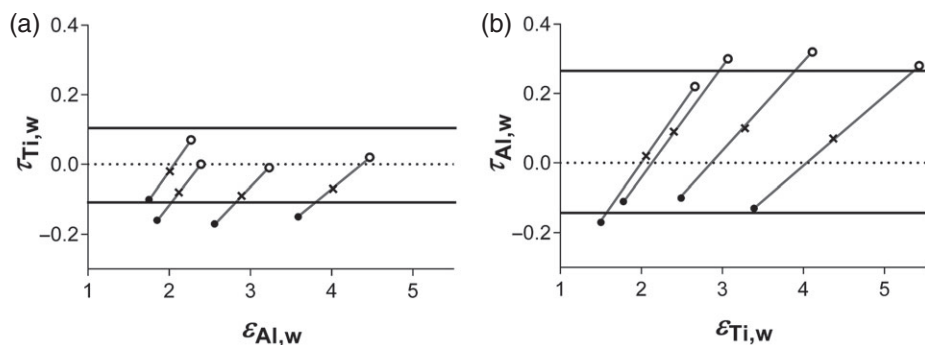
Figure 6 Transport τ (fraction, gains are positive and losses are negative) of (a) Ti and (b) Al plotted against against change in soil thickness (strain). Immobility is established when the majority of the 'transport line' connecting minimum (●), maximum (○) and average (×) strain falls within the natural variability of the immobile index element as shown by thick horizontal lines (Chadwick *et al.*, 1990).

carbon content in our model, this results in homogenized organic carbon-depth profiles.

Sensitivity of the vertical distribution of SOM to the initial thickness of the tephra deposit, which affects the degree of change in soil volume, is shown in Figure 8(c). A thicker initial current soil in the model results in dilution of the organic carbon content in the model output, which could not be corrected for by increasing organic carbon input (I_{shoots}) because the soil would then become too thick because of the increase in soil volume.
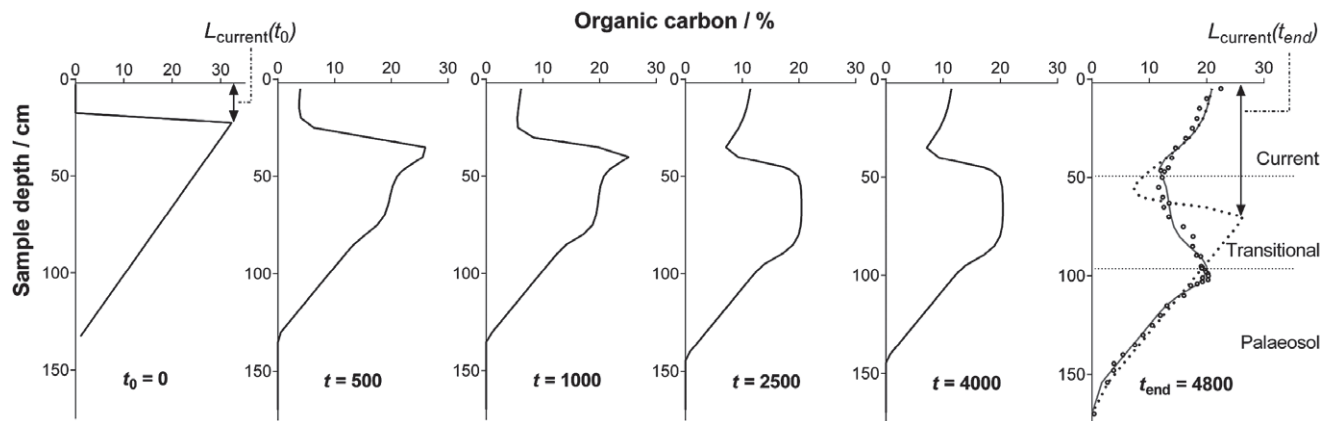
Figure 7 Modelled (–) and measured (○) organic carbon-depth profiles at several moments in time (*t* in years). The current situation is represented by the figure for $t_{end} = 4800$ years and includes also a modelled organic carbon-depth profile without bioturbation B (····). The initial total thickness of the current soil (i.e. $L_{current}(t_0)$) is indicated in the figure by t_o and its total thickness after soil formation (i.e. $L_{current}(t_{end})$) is indicated in the figure by t_{end}. We included the fit for the optimal parameter set only and not the range of the SCEM fits for clarity.
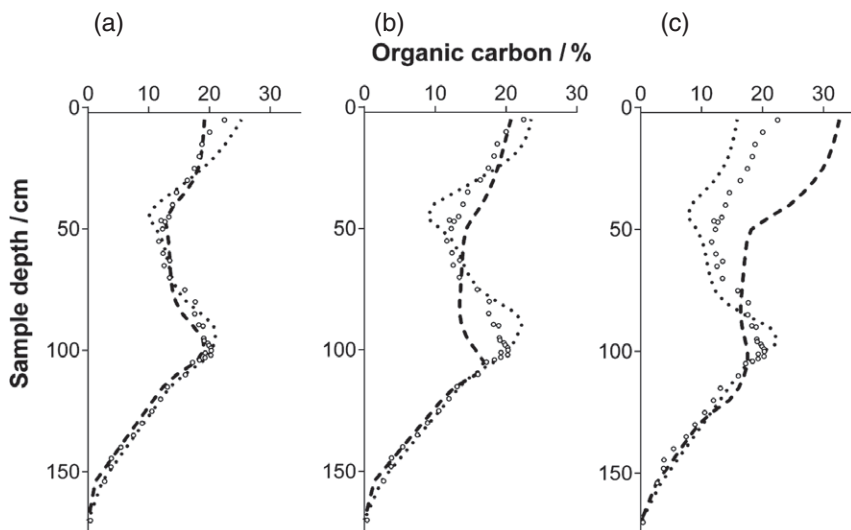
Figure 8 Modelled organic carbon-depth profiles and measured (○) organic carbon-depth profiles obtained with (a) $w_A = 56\,cm^{-1}$ (optimal fit) and $D_A = 3\,cm^2\,year^{-1}$ (- - -) or $0.3\,cm^2\,year^{-1}$ (····), (b) $D_A = 1.0\,cm^2\,year^{-1}$ (optimal fit) and $w_A = 130\,cm$ (····) or $18\,cm$ (- - -) and (c) a total initial thickness of the current soil of $30\,cm$ (····) or $10\,cm$ (- - -). Other parameter settings in these figures are equivalent to the optimal fit within the SCEM ranges presented in Table 3.

Discussion

Volume change as a major soil-forming process

The current soil more than tripled in thickness over time through incorporation of organic matter, which confirms that volume change is a major soil-forming process in the volcanic ash soil studied. Barois *et al.* (1998) also mentioned soil thickening in combination with the accumulation of SOM in Mexican Andosols, but did not quantify it. Because a large accumulation of SOM is characteristic for volcanic ash soil (Dahlgren *et al.*, 2004), we expect that soil thickening is an important process for this soil type in general. Change in soil volume might also be relevant in other types of soil that are characterized by organic matter accumulation and bioturbation, such as Chernozems and Phaeozems.

Other common soil-forming processes did not have a large effect on the volume of the soil studied. First, bioturbation itself did not necessarily lead to an increase in porosity (Tonneijck & Jongmans, 2008) and therefore could not explain the substantial thickening. Second, collapse of the soil from the leaching of elements did not seem to counterbalance the thickening, even though weathering of volcanic ash soil under perudic conditions is rapid. This may be explained by the complexation of elements with SOM (e.g. Al, Fe) and by biocycling of elements (e.g. Si, K, P), which prevent leaching. Aluminium was indeed demonstrated to be immobile.

Effect of volume change on vertical SOM distribution

In our modelling exercise, change in soil volume caused the active bioturbation zone to move upwards gradually relative to the soil base (Figure 1). The effect of such a moving bioturbation zone on the vertical distribution of SOM becomes apparent when one focuses on the observed and modelled atypical increase in SOM from the subsoil of the current soil to the top of the palaeosol (Figure 7). Although bioturbation B covered only a small distance of 5–20 cm at any moment in time (1σ bioturbation kernel), it still affected a zone of ~50 cm wide throughout the entire modelled time-frame because of this gradual move upwards. Endogeic soil faunal species, such as those represented by bioturbation B in the model, are known to create extensive horizontal burrowing networks that result in the transport of SOM over short vertical distances only (Anderson, 1988; Lee & Foster, 1991).

Bioturbation rates (represented by diffusion constants) were smaller than those estimated by Elzein & Balesdent (1995) and Van Dam *et al.* (1997). They might be small because of the unfavourable soil environment (i.e. perudic conditions and acidic pH). These small rates of bioturbation do not necessarily conflict with the abundance of bioturbation features observed by micromorphological techniques throughout the entire current soil profile (Tonneijck & Jongmans, 2008) because we now understand that these features are the cumulative result of an upwardly moving bioturbation zone.

In our model, the active rooting zone also moves upwards gradually in response to soil thickening, similar to the active bioturbation zone. The upwards shifting might explain the apparent paradox of the abundance of root-derived organic molecules such

as suberin throughout the entire 77-cm-thick current soil profile (Nierop *et al.*, 2007), whereas most roots currently occur only in the upper 10 cm according to both field and micromorphological observations (Tonneijck & Jongmans, 2008).

Lastly, an upwardly moving active bioturbation zone might help to explain the linear increase in age with depth observed in soil profiles of the study area (Tonneijck & Jongmans, 2008) because over time deeper positions become out of reach for bioturbation. Our study suggests, therefore, that palaeoecological variables such as pollen and biomarkers used to reconstruct the vegetation history (Moscol Olivera & Hooghiemstra, 2010; Jansen *et al.*, 2013) are probably distributed in a crude chronostratigraphic order in spite of bioturbation.

Evaluation of model plausibility and sensitivity

Automated parameter identification with the SCEM showed good convergence and provided posterior parameter values that were clearly within plausible ranges and did not end at the boundaries of the initial prior ranges. This enhances the confidence we can have that the dynamic model is based on a plausible concept. The model is sensitive to the rate of bioturbation (Figure 8(a)) and to changes in the initial thickness of the current soil (Figure 8(c)), which show that bioturbation and changes in volume have a large effect on the vertical distribution of SOM and need to be taken into account.

The good fit between measured and modelled vertical SOM distribution confirms (*sensu* Oreskes *et al.*, 1994) that change in soil volume may affect the vertical distribution of soil organic matter through its effect on depth-dependent processes such as bioturbation. Although this does not necessarily prove that our mechanistic process description is valid, we do show that it is plausible.

Conclusions

Our results show that change in soil volume is a major soil-forming process in volcanic ash soil. Accumulation of organic matter resulted in more than a tripling of initial soil thickness within 4800 years, from ~20 to 77 cm. Our modelling exercise shows clearly that change in soil volume affects depth-dependent soil-forming processes such as bioturbation and rooting. Therefore, volume change should be taken into account when one models and interprets organic carbon dynamics in soil, especially in the case of organic-rich soil.

Acknowledgements

References

Anderson, J.M. 1988. Invertebrate-mediated transport processes in soils. *Agriculture, Ecosystems & Environment*, **24**, 5–19.

Aran, D., Gury, M. & Jeanroy, E. 2001. Organo-metallic complexes in an Andosol: a comparative study with a Cambisol and Podzol. *Geoderma*, **99**, 65–79.

Bakker, J., Moscol Olivera, M. & Hooghiemstra, H. 2008. Holocene environmental change at the upper forest line in northern Ecuador. *Holocene*, **18**, 877–893.

Barois, I., Dubroeucq, D., Rojas, P. & Lavelle, P. 1998. Andosol-forming process linked with soil fauna under the perennial grass *Mulhembergia macroura*. *Geoderma*, **86**, 241–260.

Batjes, N.H. 1996. Total carbon and nitrogen in the soils of the world. *European Journal of Soil Science*, **47**, 151–163.

Blanco-Canqui, H., Lal, R., Post, W.M., Izaurralde, R.C. & Shipitalo, M.J. 2006. Organic carbon influences on soil particle density and rheological properties. *Soil Science Society of America Journal*, **70**, 1407–1414.

Brimhall, G.H. & Dietrich, W.E. 1987. Constitutive mass balance relations between chemical composition, volume, density, porosity, and strain in metasomatic hydrochemical systems: results on weathering and pedogenesis. *Geochimica et Cosmochimica Acta*, **51**, 567–587.

Chadwick, O.A., Brimhall, G.H. & Hendricks, D.M. 1990. From a black to a gray box – a mass balance interpretation of pedogenesis. *Geomorphology*, **3**, 369–390.

Dahlgren, R., Saigusa, M. & Ugolini, F. 2004. The nature, properties and management of volcanic soils. *Advances in Agronomy*, **82**, 113–182.

Douglas, E. & McKyes, E. 1978. Compaction effects on the hydraulic conductivity of a clay soil. *Soil Science*, **125**, 278–282.

Elzein, A. & Balesdent, J. 1995. Mechanistic simulation of vertical distribution of carbon concentrations and residence times in soils. *Soil Science Society of America Journal*, **59**, 1328–1335.

FAO 2006. *World Reference Base for Soil Resources 2006. A Framework for International Classification, Correlation and Communication*. World Soil Resources Reports No 103, FAO/ISRIC/IUSS, Rome.

Heimovaara, T.J., Huisman, S.A., Vrugt, J.A. & Bouten, W. 2004. Obtaining the spatial distribution of water content along a TDR probe using the SCEM-UA Bayesian inverse modelling scheme. *Vadose Zone Journal*, **3**, 1128–1145.

Hofstede, R.G.M. & Rossenaar, A.J.G.A. 1995. Biomass of grazed, burned and undisturbed páramo grasslands, Colombia. II root mass and aboveground:belowground ratio. *Arctic and Alpine Research*, **27**, 13–18.

Jansen, B., de Boer, E.J., Cleef, A.M., Hooghiemstra, H., Moscol-Olivera, M., Tonneijck, F.H. *et al.* 2013. Reconstruction of late Holocene forest dynamics in northern Ecuador from biomarkers and pollen in soil cores. *Palaeogeography Palaeoclimatology Palaeoecology*, **386**, 607–619.

Jarvis, N.J., Taylor, A., Larsbo, M., Etana, A. & Rosén, K. 2010. Modelling the effects of bioturbation on the re-distribution of 137Cs in an undisturbed grassland soil. *European Journal of Soil Science*, **61**, 24–34.

Jenkinson, D.S., Poulton, P.R. & Bryant, C. 2008. The turnover of organic carbon in subsoils. Part 1. Natural and bomb radiocarbon in soil profiles from the Rothamsted long-term field experiments. *European Journal of Soil Science*, **59**, 391–399.

Jobbágy, E.G. & Jackson, R.B. 2000. The vertical distribution of soil organic carbon and its relation to climate and vegetation. *Ecological Applications*, **10**, 423–436.

Lal, R. 2004. Soil carbon sequestration to mitigate climate change. *Geoderma*, **123**, 1–22.

Lee, K.E. & Foster, R.C. 1991. Soil fauna and soil structure. *Australian Journal of Soil Research*, **29**, 745–775.

Moscol Olivera, M.C. & Hooghiemstra, H. 2010. Three millennia upper forest line changes in northern Ecuador: pollen records and altitudinal vegetation distributions. *Review of Palaeobotany & Palynology*, **163**, 113–126.

Myers, N., Mittermeier, R.A., Mittermeier, C.G., da Fonseca, G.A.B. & Kent, J. 2000. Biodiversity hotspots for conservation priorities. *Nature*, **403**, 853–858.

Nierop, K.G.J., Tonneijck, F.H., Jansen, B. & Verstraten, J.M. 2007. Organic matter in volcanic ash soils under forest and páramo along an Ecuadorian altitudinal transect. *Soil Science Society of America Journal*, **71**, 1119–1127.

Oreskes, N., Shrader-Frechette, K. & Belitz, K. 1994. Verification, validation, and confirmation of numerical models in the Earth sciences. *Science*, **263**, 641–646.

Rühlmann, J., Körschens, M. & Graefe, J. 2006. A new approach to calculate the particle density of soils considering properties of the soil organic matter and the mineral matrix. *Geoderma*, **130**, 272–283.

Salvador-Blanes, S., Minasny, B. & McBratney, A.B. 2007. Modelling long-term *in situ* soil profile evolution: application to the genesis of soil profiles containing stone layers. *European Journal of Soil Science*, **58**, 1535–1548.

Soil Survey Staff 2015. *Illustrated Guide to Soil Taxonomy*, Version 2. U.S. Department of Agriculture, Natural Resources Conservation Service, National Soil Survey Center, Lincoln, NE.

Tonneijck, F.H. 1999. *Carbon Fixation in the Soil – Volcanic Soils in the Tropical Environments of Ecuador. Model Concept and Field Study*. Student Report, University of Amsterdam, Amsterdam and Quito.

Tonneijck, F.H. & Jongmans, A.G. 2008. The influence of bioturbation on the vertical distribution of soil organic matter in volcanic ash soils: a case study in northern Ecuador. *European Journal of Soil Science*, **59**, 1063–1075.

Tonneijck, F.H., Hageman, J.A., Sevink, J. & Verstraten, J.M. 2008. Tephra stratification of volcanic soils in Northern Ecuador. *Geoderma*, **144**, 231–247.

Torn, M.S.S., Trumbore, E., Chadwick, O.A., Vitousek, P.M. & Hendricks, D.M. 1997. Mineral control of soil organic carbon storage and turnover. *Nature*, **389**, 170–173.

Van Dam, D., Van Breemen, N. & Veldkamp, E. 1997. Soil organic carbon dynamics: variability with depth in forested and deforested soils under pasture in Costa Rica. *Biogeochemistry*, **39**, 343–375.

Van Reeuwijk, L.P. 2002. *Procedures for Soil Analysis*, 6th edn. Technical paper. ISRIC, Wageningen.

Vrugt, J.A., Gupta, H.V., Bouten, W. & Sorooshian, S. 2003. A Shuffled complex evolution metropolis algorithm for optimization and uncertainty assessment of hydrologic model parameters. *Water Resources Research*, **39**, 1201.